Thermochimica Acta
Elsevier Publishing Company, Amsterdam
Printed in Belgium

PHENOLIC RESIN CHAR-FORMATION DURING HYPERTHERMAL ABLATION*

R. W. FARMER
Air Force Materials Laboratory, Wright–Patterson AFB, Ohio 45433 (U. S. A.)
(Received March 11th, 1972)

ABSTRACT

Ablation is a self-regulating heat and mass transfer process in which incident thermal energy is expended by sacrificial loss of material**.

The surface of a carbonaceous char is lost during the ablation of fiber-reinforced phenolic resin composites. The transient high temperatures penetrate deeply, resulting in an underlying pyrolysis zone with rapid pyrolysis rates and a high char interface temperature.

Phenolic resin char-formation at high heating rates and high temperatures was studied using thermogravimetry (TG). The specialized thermobalance permitted runs in helium at rates of 3–430°C/min up to 1400°C.

Computer code analysis provided rate parameters for an Arrhenius type correlation. The parameters represented well the parent TG run but were not independent of heating rate.

A complex correlation was considered necessary for universal use. The attractive alternative was parameter evaluation at high heating rates using TG.

SYMBOLS

A	kinetic parameter, l/min
A^+	kinetic parameter, $(g/cm^3)^{1-n}$/min
A_c	cross-sectional area, cm^2
e	logarithmic base, dimensionless
E	kinetic parameter, kcal/g-mole
exp	exponential to the base e, dimensionless
f	function
k	kinetic parameter, l/min
K	integral parameter, dimensionless
L	effective length, cm
m	series term, dimensionless

*Presented before the Third Annual Meeting of the North American Thermal Analysis Society in Waco, Texas, on February 7–8, 1972.
**ASTM (E 349)30.

n	kinetic parameter, dimensionless
p	density, g/cm^3
p_{oi}	initial density, g/cm^3
p_r	residual density, g/cm^3
q	heat transfer, kcal
r	relative error, dimensionless
r_c	cylinder radius, cm
R	gas constant, kcal/g-mole/°K
$\dot{S}$	recession rate, cm/min
t	time, min
T	temperature, degrees absolute*, °K
T_1	temperature at L, °K
ΔT	(surface−center) temperature*, °K
w	residue-free basis weight fraction, dimensionless
w_s	sample weight fraction, dimensionless
w_{oi}	initial sample weight fraction, dimensionless
w_r	residual sample weight fraction, dimensionless
x_{oi}	initial sample weight, g
X	E/RT, dimensionless
$(\cdot)$	d( )/dt*, 1/min
$(\cdot)_T$	d( )/dT*, 1/°K
α	thermal diffusivity*, cm^2/min
λ	thermal conductivity, kcal/cm/min/°K
m	maximum rate of weight loss, subscript
1, 2	singular case, subscript

INTRODUCTION

The generation of fundamental kinetic, thermochemical, or other properties can usually be made without considering end-uses.

Engineering, subject to varying levels of empiricism, must insure that less-than-fundamental data are consistent with the physical environment and are known within some suitable range of confidence. An example is the semi-empirical data for ablative materials that have successfully provided thermal protection as heatshields, nosetips, and rocket nozzles in hyperthermal environments.

The complex processes in the ablation of a carbonaceous fiber reinforced phenolic resin are conveniently relegated to functional zones. The simplified model of Fig. 1 is for a "steady-state" condition of time-independent heat transfer, mass transfer, and surface recession rate.

Resin decomposition occurs in the pyrolysis zone. The composite forms a porous char consisting of fiber and the carbon from resin pyrolysis.

*Different units for a symbol are noted with that symbol.

The char surface is convectively heated by the surrounding hot gas flow field. Radiative exchange also occurs between the char and gas.

There is diffusive mass transfer of chemically reactive species to the surface from the boundary-layer, pyrolysis zone, and char zone. Additional diffusion occurs for the products of reactions between the hot gas, char, and pyrolytic gas.

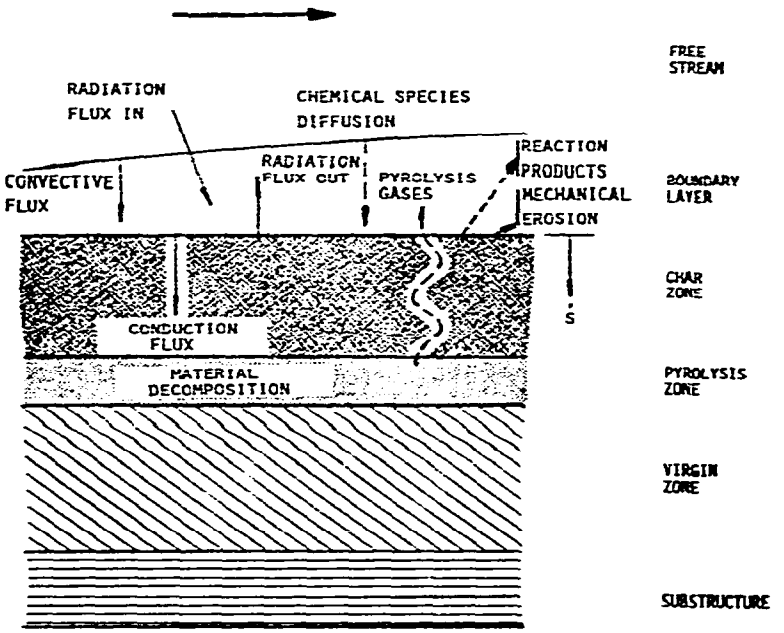

Fig. 1. Heat and mass transfer mechanisms.

Heat transfer within the char can involve chemical, conductive, diffusive, and radiative elements. Low total conduction efficiently cools the substructure and underlying components.

Mechanically-induced surface recession may result under sufficiently severe combinations of heating, pressure, and shear.

As illustrated by Fig. 2, the gas pressure and temperature gradients are ideally continuous through the char and pyrolysis zones. There is a density discontinuity at the high temperature interface with a sharp gradient across the pyrolysis zone.

Density kinetics in the pyrolysis zone are frequently expressed in an empirical Arrhenius-type correlation, such as

$$-\dot{p} = A^{+}(p-p_r)^{n} \exp -E/RT \qquad (1)$$

These correlations are widely used in materials study and design applications. Other input properties for the analytical model, such as permeability, specific heat, or thermal conductivity, may further be taken as a function of the local density or the local temperature as calculated from the relation.

The empirical kinetic parameters n, A^{+}, and E are frequently derived from

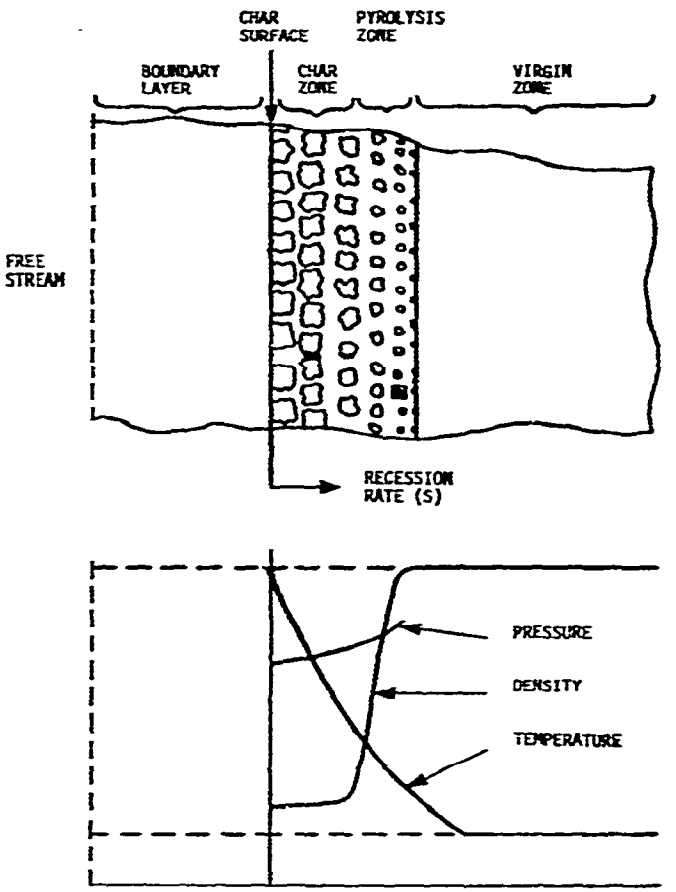

Fig. 2. Steady-state profiles in the pyrolysis zone.

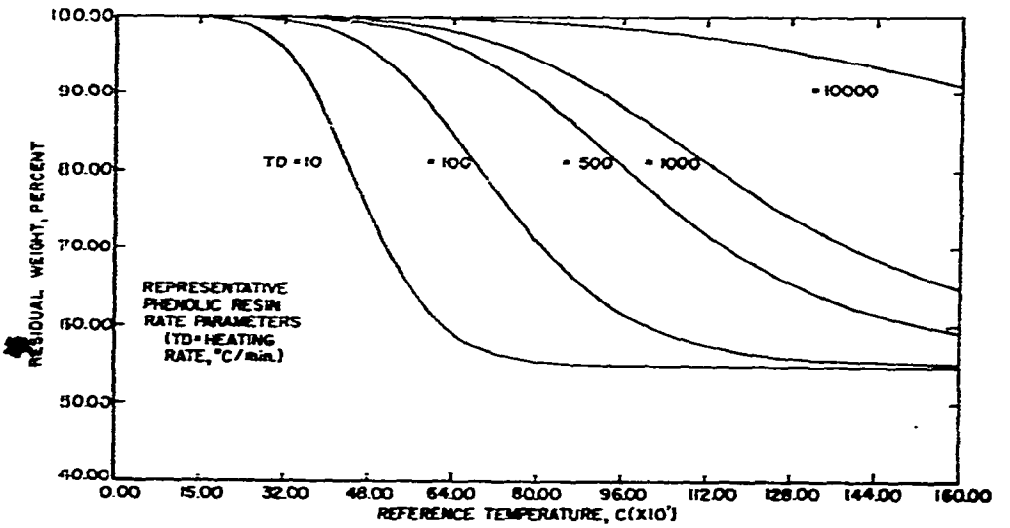

Fig. 3. Weight profiles for a constant pyrolysis zone heating rate.

thermogravimetry (TG) experiments at heating rates of 10°C/min or so. The mean pyrolysis zone rates, however, may be from 10 to 2000 times larger.

Fig. 3 illustrates the temperature dependence of pyrolysis zone resin weight as a function of mean heating rate. This extrapolation of kinetic parameters was invalid. Large char yields have not been found for specimens subjected to either very high heating rates or to hyperthermal ablation.

To better understand and to express phenolic resin char-formation, a TG study was made to a temperature typical of that of the char and pyrolysis zone interface. Computer code analysis provided baseline rate parameters for a low heating rate.

Additional experiments were run at heating rates up to practical limits on apparatus and probable experimental error. Derived parameters were compared with the low heating rate results.

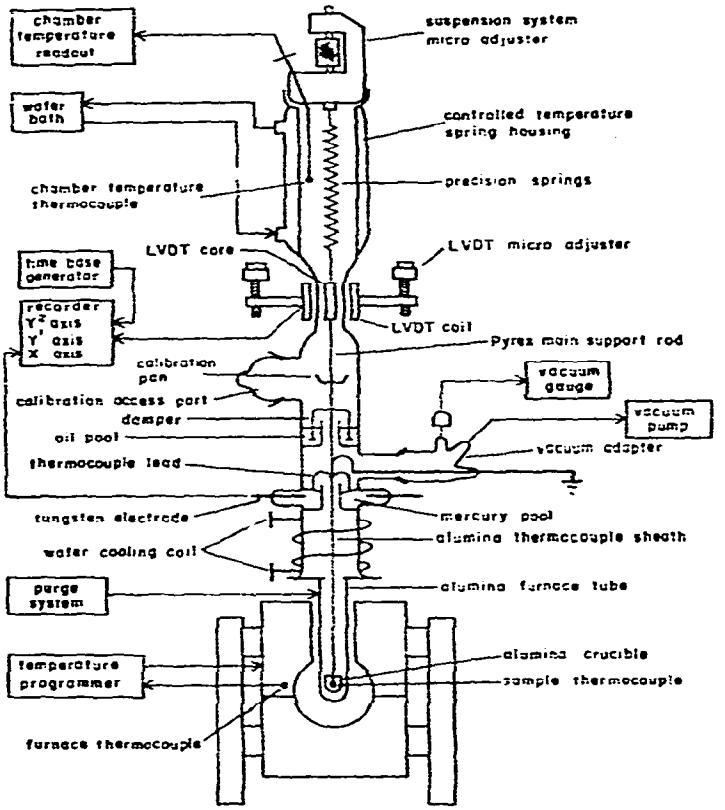

Fig. 4. Diagram of the recording thermobalance.

EXPERIMENTAL

Recording thermobalance

The modified Aminco Thermo-Grav recording thermobalance is illustrated in Fig. 4. A weight–temperature–time curve was automatically plotted by an $X–Y^1–Y^2$ recorder. During the run a change in sample weight caused two precision springs to

move. A linear variable differential transformer (LVDT) response voltage drove one recorder pen. A platinum–platinum +13% rhodium–platinum (ground) thermocouple produced the emf to move the X-axis carriage. Run time was plotted by the Y^2 pen by means of a synchronous time-base generator.

The Pyrex support rod was joined to the springs just below the housing. The rod held an LVDT core, weight pan, and an oil dashpot ring. The crucible, thermocouple, and alumina sheath hung from the rod into the furnace.

The sample thermocouple signal was grounded and filtered to shield against noise pickup at high temperatures. The feedthroughs (fine tungsten-wire lead–mercury pool–tungsten electrode) had little mechanical effect upon spring linearity.

The original tubular crucible (McDanel Refractory Porcelain Company body AP35 recrystallized alumina) was 0.25 in. inside diameter, 0.375 in. outside diameter, and 1 in. long. The crucible was ground to give two lobes and a remaining 0.5 in. of outside length. For support, an alumina pin was placed through a hole in each of the opposing lobes and a hole in the sheath.

The spherical furnace (Tem-Press Research, Inc., Model SQ-IC-4) was controlled by an SCR power programmer (F & M Model 240M). A strip chart recorder (Leeds and Northrup) plotted a temperature–time history for the Pt–Pt+10% Rh control thermocouple. The 1-in. outside diameter, 9.5-in. furnace tube was made of alumina (McDanel body AP35).

In addition to a controlled temperature spring housing, there were water cooling provisions for the furnace periphery and the three mercury pools.

The exploratory high heating rate experiments were conducted using another version of the thermobalance. The weight–temperature curve was automatically plotted by an X–Y recorder. A time–temperature curve was plotted by a separate high speed, strip chart recorder.

With reference to Fig. 4, essentially the same suspended components were involved using a simple Pyrex–Vycor envelope. Micro adjustors, a spring housing, or sample thermocouple electrodes were not used.

The well-oxidized Inconel crucible (Stone Type SH-1-9A(IN)) was about 0.77 cm in diameter and 1 cm in length. The crucible was hung from the central support rod with a Chromel wire.

An identical "dummy" crucible was placed immediately below the sample crucible. A 1.6-mm outside diameter, Chromel–alumel, Inconel-sheath thermocouple was bonded with ceramic cement in the bottom, inner annulus of the dummy. The thermocouple was used to drive the X–Y and strip chart recorders.

The furnace (RI Controls Type E2-10) was essentially a dual ellipsoidal "clam shell". Radiant heating was provided by tubular quartz, tungsten filament infrared lamps (GE Type 2000T3/CL/HT) located at the two foci. The crucibles and holders were aligned along the vertical focal axes of the polished aluminum reflectors.

The furnace was controlled by an SCR power supply (RI Controls Model SPG50009A). With some adjustment, a wide range of nearly linear heating rates were possible by simply firing at a selected control voltage. The heating rate curve and a

reference curve were visually monitored during the run. Minute voltage corrections were manually applied as necessary.

The furnace tube was a length of 30 mm outside diameter glass tubing (Vycor). It was held in place with a modified tube fitting (Swagelok).

Standard run

For the low heating rate work, a −325 sieve, dried powder was run at 8.5 °C/min to 1400 °C in a helium purge flowing at an inlet rate of 1 liter/min.

The calibrated X–Y^1–Y^2 recorder ranges were 0–20 mg/5 in., 0–16 mV/20 in., and 0–200 min/5 in., respectively. This ordinate corresponded to a span of 50% of the original 40-mg sample. The abscissa was convertible to a non-linear reference temperature span of 0–1402 °C. The reciprocal slope of the run time curve was the heating rate.

Two recorder sweeps were made to improve precision. To do this, the carriage was manually shifted back to zero after 10 in. of travel (to 806 °C) to give 20 in. of chart (to 1402 °C).

There was no standard run for the high heating rate work. In general, a −325 sieve, dried powder was run to 1000 °C in a helium purge flowing at an inlet rate of 1 liter/min. A range of heating rates were examined for a sample weight of 10–20 mg.

For both low and high heating rate runs, the thermobalance was purified by three consecutive evacuation and fill cycles. The helium purge resulted from a final internal pressurization to slightly above atmospheric pressure.

Material

The phenol formaldehyde molding was prepared from a novolac resin (Monsanto Chemical Company R14009). The "as received" brown powder was about −400 sieve in particle size.

The molding was made in a small stainless-steel jig. The loaded jig was processed in a commercial press for compression molding. The conditions involved 320 p.s.i. for 30 min at 92 °C with a gradual change over a 15-min period to 160 °C, which was held for 30 min.

The postcure temperatures of 150 °C and 178 °C were for 24 h each with the jig at a pressure of 320 p.s.i.

The nominal dimensions of the postcured molding were 4 in. for length, 0.125 in. for thickness, and 1 in. for width.

A lathe method of machining bulk material with a "low bite" cutter was used to prepare a fine powder. The molding was adhesively bonded to an aluminum plate for support during machining.

The sieved powder was "dried" in a small vacuum oven to reduce the free moisture content. The conditions involved 50 min at 125 °C and about 18 in. of mercury pressure.

Residue-free basis weight

The portion of the polymer available for pyrolysis was the initial-weight to char stable-weight difference. This active material was further normalized to be independent of the initial sample weight. The normalized weight fraction w

$$w = (w_o - w_r)/(w_{oi} - w_r) \tag{2}$$

was termed a "residue-free" weight fraction.

Kinetic analysis

The basis of the kinetic analysis was the isothermal relationships

$$-\dot{w} = kw^n \tag{3}$$

$$k = A \exp -X \tag{4}$$

as expressed in terms of the residue-free basis weight.

For applications to the ablative char zone, a constant volume element was generally assumed. For example, for Eqn. (1), the resulting relationship between A^+ and A was

$$A^+ = A\, p_{oi}^{(1-n)}\, x_{oi}^n\, (x_{oi} - w_r x_{oi})^{-n} \tag{5}$$

where x_{oi} and p_{oi} were the initial sample weight and material density, respectively.

An equivalent constant heating rate relation for Eqns. (3) and (4) was

$$-\dot{w}_T = (w^n A/\dot{T}) \exp -X \tag{6}$$

and was rearranged as

$$K = -\int_1^w w^{-n}\, dw \tag{7}$$

$$= (A/\dot{T}) \int_0^T e^{-X}\, dT \tag{8}$$

where K was a convenient functional symbol.

Integration of Eqn. (8) by parts in two different ways gave

$$K = (AE/R\dot{T})\, p(X) \tag{9}$$

$$p(X) = X^{-1} e^{-X} - \int_x^\infty X^{-1} e^{-X}\, dX \tag{10}$$

$$K = (AE/R\dot{T}) \left[1 - \sum_m (-1)^{m+1} X^{-m} (m+1)!\right] X^{-2} e^{-X} \tag{11}$$

For $m = 0$, a relative error r was defined for the ratio of Eqns. (9) and (10) as

$$r = X^2 e^X p(X) \tag{12}$$

and gave an additional useful expression for K

$$K = r(AE/R\dot{T}) X^{-2} e^{-X} \tag{13}$$

The computer code, called MAXRAX for convenience, calculated an (n, A, E) set from maximum rate of weight loss experimental data. Essentially, the four relationships

$$A = (w^{1-n} \dot{T} X/nT) e^X \tag{14}$$

$$E = -\dot{w}_T nRT^2/w \tag{15}$$

$$n = (\ln(r(n^{-1}-1)+1))/\ln w + 1 \tag{16}$$

$$r = X^2 e^X p(X) \tag{17}$$

were solved by an iterative procedure further using the tabulated tables

$$r = f_1(X) \tag{18}$$

$$w = f_2(n, r) \tag{19}$$

MAXRAX resulted from a maximum rate of weight loss solution of Eqns. (3) and (4), namely, Eqn. (15). The other relations for A and n came from a comparison of Eqn. (15) with Eqns. (3), (4), and (13).

PAR 3 was a computer code for graphical construction of a curve for an (n, A, E) set. Additional inputs were w_{oi}, w_r, and $\dot{T}$.

In operation, PAR 3 first solved Eqn. (9) for K at a temperature point using a $p(X)$ table. A w value was then calculated using the solution of Eqn. (7)

$$w = e^{-K} \qquad \text{for } n = 1 \tag{20}$$

and

$$w = (K(n-1)+1)^{1/(1-n)} \qquad \text{for } n \neq 1 \tag{21}$$

The w value was then converted to the observed sample weight fraction w_o

$$w_o = w(w_{oi} - w_r) + w_r \tag{22}$$

where w_{oi}, the initial sample weight fraction, was taken as unity for a single pyrolysis mechanism.

Two X–Y plotter options of PAR 3 were used for this work. For the low heating rate runs, 199 weight fractions were plotted for 0.1-in. increments of chart from 14.4 °C to 1402.2 °C. For high heating rate cases, 199 points were used for a linear temperature scale up to 1000 °C.

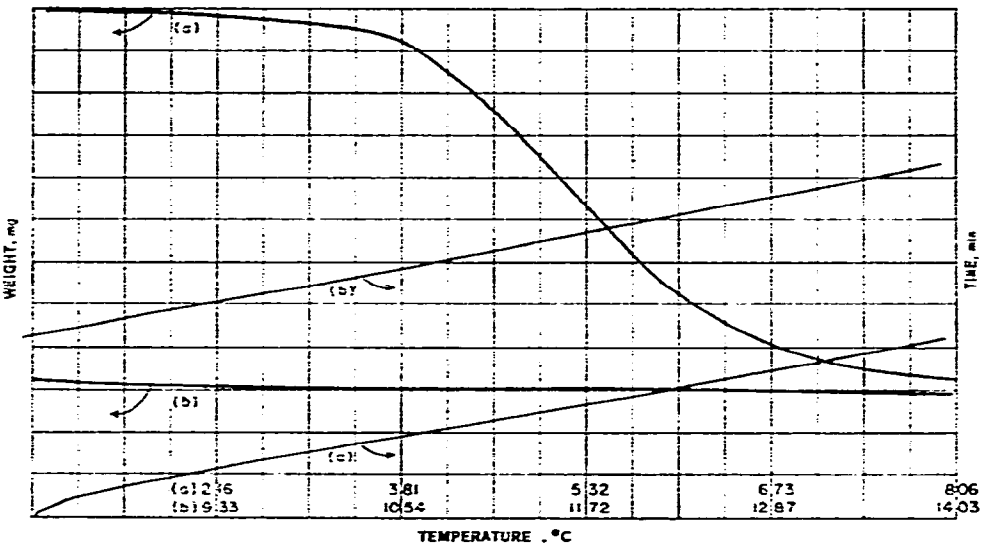

Fig. 5. Thermogram of the phenol formaldehyde molding (RI4009)

RESULTS AND DISCUSSION

Low heating rate results

The greatest weight loss portion of the curve resembled an elongated arc tangent function (Fig. 5). There was apparent pyrolysis to 1400°C. The rate beyond 806°C was small with little total weight change for the second sweep.

MAXRAX was used to calculate kinetic parameters for six replicates (Table I). There was a mutual compensation between n, A, and E. The tendency was for A and E to increase with an increase in n. This was consistent with Eqns. (15) and (14). The former showed E to be proportional to n. The latter indicated that although A was an inverse function of n, this dependence was easily outweighed by an exponential dependence upon E.

With the exception of (n, A, E), the terms remaining in Eqns. (14) and (15) were well produced on the basis of inspection and standard deviation. Slight trends, however, were still apparent. For example, w_m ideally varied with both n and r_m to nearly equal but opposite degrees. The results showed a small but still consistent increase in w_m and an increase in n with a decrease in r_m.

PAR 3 curves were plotted using the MAXRAX data and compared with the experimental ones. Fig. 6 is a representative example.

There were four regions of disagreement for the six comparisons. The calculated weights were respectively high, low, high, and low by up to 1% from 120°C to 340°C, 340°C to 380°C, 380°C to 600°C, and above 600°C.

The largest calculated–experimental weight deviation of up to 2% was just before or after the pen shift (806°C). In terms of reproducibility ,the maximum spread of 2.4% for the experimental curves was also at the pen shift.

TABLE I

MAXRAX EMPIRICAL KINETIC PARAMETERS

Parameter	*Run No.*						*Limiting values*	*Mean values*	*Standard deviation*
	500	*503*	*506*	*520*	*529*	*539*			
n	1.05845	1.19507	1.13994	1.36876	1.22478	1.24211	1.21361 ±0.15516	1.20485	0.09522
A (min^{-1})	34.9036	73.8774	71.5610	237.429	88.9396	90.8412	57.2921 ±33.5492	63.9776	8.1150
E (kcal/mole)	10.0490	11.1263	11.0672	12.7149	11.4115	11.4388	11.3820 ±1.3330	11.3013	0.7835
r_m	0.793167	0.804327	0.803748	0.819920	0.807209	0.807486	0.806543 ±0.013376	0.805976	0.000785
$\dot{T}$ (°C/min)	8.44	8.44	8.44	8.55	8.33	8.38	8.44 ±0.11	8.43	0.07
T_m (°C)	532	532	532	527	532	532	530 ±3	531	2
$\dot{T}_m$ (°C/min)	10.13	10.22	10.32	10.34	10.00	9.93	10.13 ±0.20	10.16	0.15
T_r (°C)	1400	1400	1400	1400	1400	1400	1400 ±0	1400	0
w_m	0.4589	0.4845	0.4739	0.5076	0.4888	0.4942	0.4833 ±0.0244	0.4846	0.0154
w_r	0.560	0.540	0.555	0.543	0.546	0.555	0.550 ±0.010	0.550	0.001
$-\dot{w}_{T_m}$ ($°C^{-1}$)	−0.003382	−0.003502	−0.003572	−0.003702	−0.003536	−0.003539	−0.003542 ±0.000160	−0.003539	0.000095

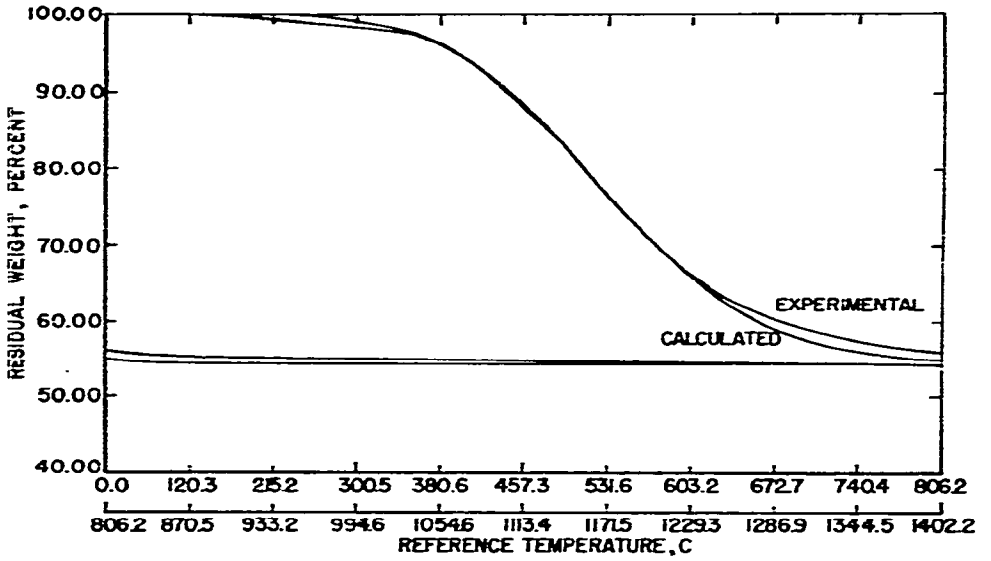

Fig. 6. Calculated and experimental curves at a low heating rate.

High heating rate results

The effect of a high heating rate was greater weight retention than for more conventional heating up to about 700°C. Less weight retention was then found with a difference ranging up to as high as 6.5% at 1000°C.

A binary pyrolysis mechanism was found at high heating rates. The discontinuity was small compared to curve readability and experimental error.

Irrespective of low precision, an analysis was made for a 430°C/min run. Considering the two steps as consecutive and independent processes as a first approximation, three cases were calculated: step 1 ending at 430°C, step 2 from 430°C to 982°C, and an average using step 2 data (Table II).

TABLE II

KINETIC PARAMETERS AT 430°C/MIN

Parameter	*High rate*			*Low rate, mean value*
	First step	*Second step*	*Average*	
n	4.13065	1.69115	0.996545	1.20485
A (min^{-1})	3.16940×10^{16}	399373	2777.9	63.9776
E (kcal/mole)	50.4525	20.1711	12.0579	11.3013
r_m	0.948107	0.860222	0.801151	0.805976
$\dot{T}$ (°C/min)	430	430	430	8.43
T_m (°C)	450	625	625	531
$\dot{T}_m$ (°C/min)	430	430	430	10.16
T_r (°C)	982	982	982	1400
w_m	0.667	0.534	0.378	0.4846
w_r	0.850	0.485	0.485	0.550
$-\dot{w}_{T_m}$ ($°C^{-1}$)	−0.00784	−0.003971	−0.002820	−0.003539

The average set of parameters gave the best fit to the experimental curve. (Fig. 7). Although the two steps did fit together fairly smoothly, the dual *vs.* experimental curve differences were overall larger than for the average *vs.* experimental curve differences.

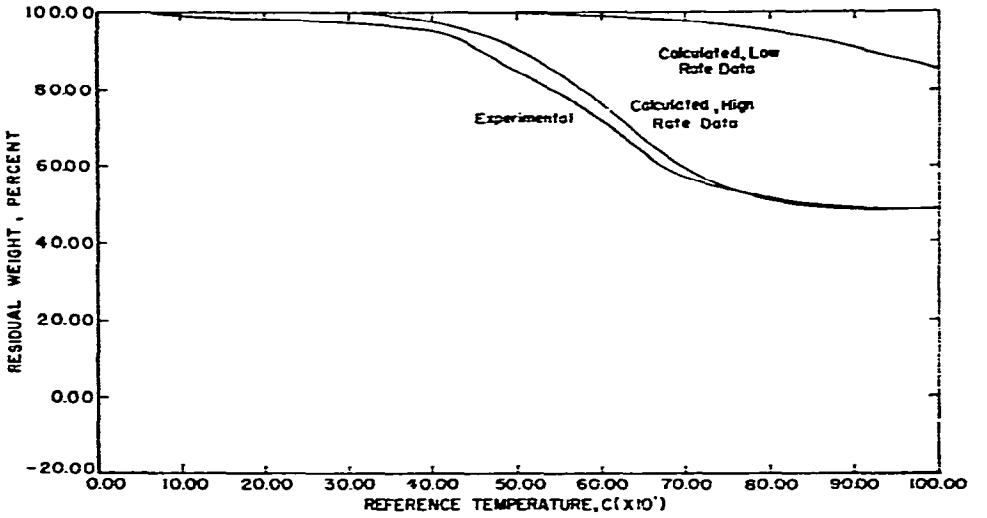

Fig. 7. Calculated curves using two methods and experimental curve at a high heating rate.

The averaged MAXRAX–PAR 3 curve was within about 6% by weight of the experimental curve. There was a long difference band from about 400 °C to 700 °C with the maximum value occuring near 500 °C.

The high heating rate curve was also calculated using the mean MAXRAX parameters from the six-run analysis (see Table I and Fig. 7). There was no agreement.

Heat and mass transfer

There were a variety of possible heat-transfer and mass-transfer errors during thermogravimetry.

Volatiles species from pyrolytic reactions were possibly aligned by normal diffusion, mutual solubility, or thermal diffusion into concentration gradients. The gradient retarded the rate of weight loss and controlled kinetically if the loss rate was less than the generation rate.

Thermal gradients within the sample and crucible further suppressed pyrolytic rates and net weight change.

Heat and mass-transfer effects may have been present but did not completely control a high heating rate run. The final zero slope within the few available seconds of run time was not consistent with true control. Further, other interactions, as the pyrolysis mechanism change plus heat and mass-transfer effects over ranges of temperature, were more consistent with the zero slope and the higher weight retention found at moderate temperatures for a low rate of heating.

A preliminary assessment was made of temperature uncertainty. A recording radiometer (Radiation Electronics Thermodot Model TD-6AG) was focused through a sodium chloride window into the dummy crucible. The magnified field-of-view was the capped end of the annular tube occupied by the bonded thermocouple.

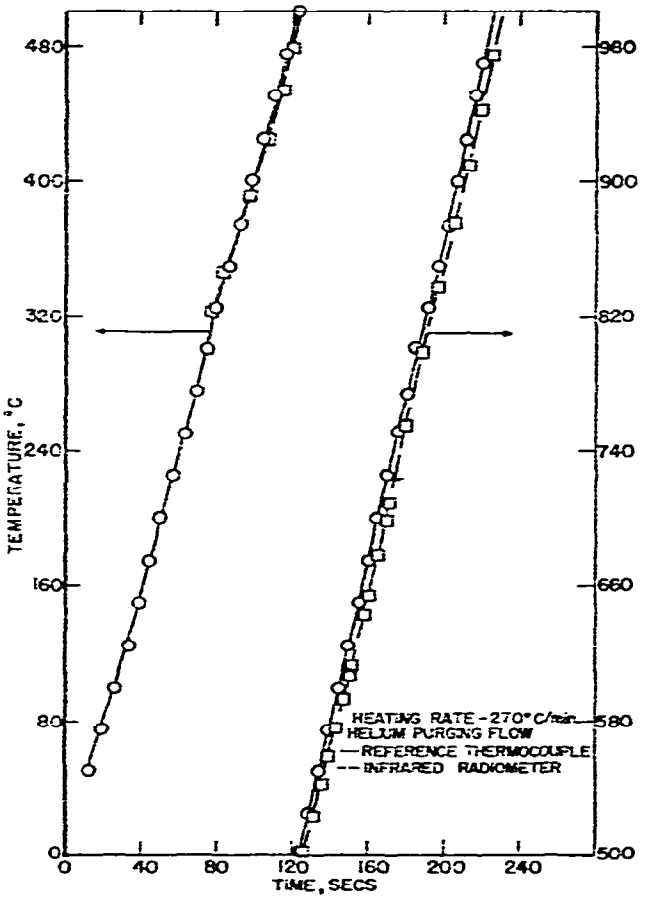

Fig. 8. Reference thermocouple and radiometer heating curves.

A low temperature was found for the radiometer for a wide range of heating rates. As illustrated by Fig. 8, the difference gradually increased with time, approaching 30 °C near 1000 °C. The radiometer was ineffective below 320 °C.

There was a radiometric error due to window absorption and the crucible emittance. Using a spectrophotometer (Perkin-Elmer IR5-A), average transmittance and reflectance values of 0.94 and 0.07 were measured for the window and an oxidized Inconel plate, respectively. The spectral region was from 3.5 to 4.1 microns to correspond to the spectral response of the radiometer. The measurements were made at room temperature.

Using the spectral data and conventional theory, a maximum 20 °C low-radiometric error was calculated at 1000 °C. Therefore, it was possible that the minimum

and maximum temperature uncertainties were no more than 10°C and 30°C, respectively.

The radiometer and thermocouple sensed a mean temperature for the annular tube of the crucible. To further assess radial gradients, calculations were made for a solid infinite cylinder. At long time, the temperature difference ΔT between the surface and center of the cylinder approached

$$\Delta T = \dot{T} r_c^2 / 4\alpha \tag{23}$$

where $\dot{T}$ was the surface heating rate.

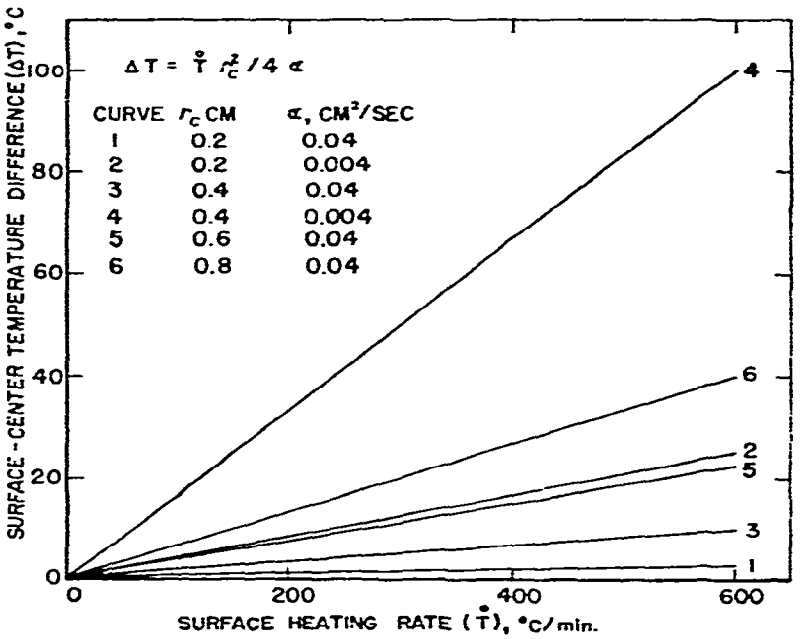

Fig. 9. Thermal gradient for an infinite cylinder.

Calculations were made for thermal diffusivity values representative for char (0.4 cm^2/sec), Inconel (0.04 cm^2/sec), phenolic resin (0.001 cm^2/sec), and a carbonaceous fiber reinforced phenolic resin (0.004 cm^2/sec) for cylinder radii of 0.2–1.0 cm (Fig. 9). The results showed that a high diffusivity and a small radius were desirable for a minimum radial gradient.

The solid infinite cylinder was a conservative, ideal case. From a practical viewpoint, the double-shell crucible, moderate convective heat loss at low temperature, and large radiative loss at high temperature would generally be expected to give a lower thermal gradient.

A lateral thermal gradient was possible along the crucible and the thermocouple sheath. The crucible received less energy as a result of diameter difference, materials properties, and the variation in field intensity.

A low thermal conductivity for the crucible and sheath together with small

physical dimensions were desirable to reduce a lateral gradient. For example, the conductive heat gain by the crucible occurred approximately as

$$q = A_c\lambda\int_{t_1}^{t_2}(T_1 - T_c)\,dt/L \tag{24}$$

for mean values of cross-sectional area (A_c), thermal conductivity (λ), and temperature gradient length (L).

The magnitude of possible mass-transfer errors could not be easily assessed. It was apparent, however, that a physically small sample with a large free area and good gaseous interchange with the environment was desirable. These goals were further generally consistent with the reduction of possible heat-transfer error.

CONCLUSIONS

Char-formation at 8.5 °C/min to 1400 °C was represented by rate parameters for an Arrhenius-type correlation.

Heating rate was an explicit term in the correlation. Further exploratory runs were made to 430 °C/min. The rate parameters were not independent of heating rate.

Heat- and mass-transfer errors were not overwhelmingly large at high heating rates.

Careful equipment design should permit accurate study of correlations and parameters for a wide range of heating rates.